

Article

# Optimising Ion Conductivity in NdBaInO<sub>4</sub>-Based Phases

Manyu Chen <sup>1,\*</sup> , Cheng Li <sup>2</sup> , Kai Zhu <sup>1</sup>, Jieyu Wang <sup>1</sup>, Sida Liu <sup>1</sup>, Weina Kong <sup>1</sup>, Zifa Ban <sup>1</sup> and Chao Shen <sup>1</sup><sup>1</sup> Avic Composite Corporation Ltd., Beijing 101300, China<sup>2</sup> Neutron Scattering Division, Oak Ridge National Lab, Oak Ridge, TN 37831, USA

\* Correspondence: chenmanyu025@163.com; Tel.: +86-18911985291

**Abstract:** Based on the previous work conducted by Fujii et al., NdBaInO<sub>4</sub> compounds present modest oxide-ion conductivities. Therefore, it has been an attractive system of significant interest. In this study, we attempted to partially substitute Ca for Nd and the total electrical conductivity was successfully improved due to the generation of oxygen vacancies. The synthesis, crystal structure, density, surface topography, and electrical properties of NdBaInO<sub>4</sub> and Ca-doped NdBaInO<sub>4</sub> have been studied, respectively. NdBaInO<sub>4</sub> and 10% and 20% molar fractions of Ca-doped NdBaInO<sub>4</sub> were synthesized through solid-state reactions. The crystal structure of them was obtained from Le Bail refinement of the XRD pattern, giving the result of the monoclinic structure, which belongs to P2<sub>1</sub>/c space group. The highest total electrical conductivity of  $4.91 \times 10^{-3} \text{ S cm}^{-1}$  was obtained in the Nd<sub>0.9</sub>Ca<sub>0.1</sub>BaInO<sub>3.95</sub> sample at a temperature of 760 °C in the dry atmosphere and the activation energy was reduced from 0.68 eV to 0.58 eV when the temperature was above 464 °C (737 K) after doping the NdBaInO<sub>4</sub> with a 0.1 molar fraction of Ca<sup>2+</sup>. Moreover, the total conductivity of Nd<sub>0.9</sub>Ca<sub>0.1</sub>BaInO<sub>3.95</sub> in the wet atmosphere at moderate temperature was relatively higher than that in the dry atmosphere, which suggests that potential proton conduction may exist in wet atmospheres. In addition, the oxygen diffusion coefficients of Nd<sub>0.9</sub>Ca<sub>0.1</sub>BaInO<sub>3.95</sub> ( $D^* = 1.82 \times 10^{-8} \text{ cm}^2/\text{s}$ , 850 °C) was about two times higher than that of Nd<sub>0.8</sub>Ca<sub>0.2</sub>BaInO<sub>3.90</sub> ( $D^* = 7.95 \times 10^{-9} \text{ cm}^2/\text{s}$ , 850 °C) and was increased significantly by two orders of magnitude when compared with the oxygen diffusion coefficient of the undoped NdBaInO<sub>4</sub> ( $D^* = 8.25 \times 10^{-11} \text{ cm}^2/\text{s}$ , 850 °C).

**Keywords:** Ca-doped NdBaInO<sub>4</sub>; oxide-ion conductivities; electrical conductivity; activation energy; proton conduction; oxygen diffusion coefficients



**Citation:** Chen, M.; Li, C.; Zhu, K.; Wang, J.; Liu, S.; Kong, W.; Ban, Z.; Shen, C. Optimising Ion Conductivity in NdBaInO<sub>4</sub>-Based Phases. *Energies* **2024**, *17*, 2029. <https://doi.org/10.3390/en17092029>

Academic Editor: Vladislav A. Sadykov

Received: 11 February 2024

Revised: 18 April 2024

Accepted: 22 April 2024

Published: 25 April 2024



**Copyright:** © 2024 by the authors. Licensee MDPI, Basel, Switzerland. This article is an open access article distributed under the terms and conditions of the Creative Commons Attribution (CC BY) license (<https://creativecommons.org/licenses/by/4.0/>).

## 1. Introduction

Solid oxide materials with high oxide-ion conductivity and proton conductivity have been widely applied to many technological applications such as oxygen separation membranes, PCECs, and solid oxide fuel cells (SOFCs) [1–10], thus they have attracted a great deal of interest. The most investigated oxygen-ion and proton conductors are complex oxides with perovskite structures. A perovskite-related structure family with monoclinic P2<sub>1</sub>/c phase and AA'BO<sub>4</sub> composition, which is based on NdBaInO<sub>4</sub>, has been reported by Fujii et al. [11]. It is an oxide-ion conductor, but the ionic conductivity is relatively modest. Therefore, many investigations have been carried out on this structure.

The transport properties in ceramic oxides are dominated by type, concentration, and mobility of charge carriers in the materials. Therefore, not only the crystal structure but also the defects, point defects in particular, have dramatic effects on the oxide-ion conductivity of the material. There are two types of defects in solid oxides, one is intrinsic defects and another is extrinsic defects. Extrinsic defects are mainly influenced by some external factors such as temperature, oxygen partial pressure, and doping elements. Doping effects have the benefit of promoting the charge carriers' concentration, which improves electrical conductivity. Therefore, it is practicable to chemically modify the composition of NdBaInO<sub>4</sub> to enhance oxide-ion conductivity, which can be realized by introducing oxygen vacancies into NdBaInO<sub>4</sub> through doping with aliovalent cations.

Fujii et al. [12] successfully doped Sr at the Nd site and the electrical conductivity was significantly improved due to the increase in the concentration of oxygen vacancies, which act as carriers for oxide-ion conduction. In addition, the activation energy was reduced through doping with Sr. It was also found by Ishihara et al. [13] that the substitution of In with Ti in NdBaInO<sub>4</sub> is effective for increasing oxide-ion conductivity.

In this work, we attempted to partially substitute a small amount of Ca element for Nd, which has the potential to improve the total electrical conductivity and decrease the activation energy by introducing oxygen vacancies. The crystal structure and lattice parameters of Ca-doped NaBaInO<sub>4</sub> were characterized via X-ray diffraction and Le Bail refinement. The electrical conductivity of Ca-doped NaBaInO<sub>4</sub> was measured through AC impedance spectroscopy. The properties of NaBaInO<sub>4</sub> were also analysed for comparison. Furthermore, the effects of Ca<sup>2+</sup> doping on the electrical properties and the mechanism of the ion diffusion were studied and are discussed in this work.

The rest of this paper is organized as follows. In Section 2, we present the details of the synthesis procedure and general analytical methods. Then, the crystal structure, density, surface topography, and electrical properties of NdBaInO<sub>4</sub> and Ca-doped NdBaInO<sub>4</sub> have been studied, respectively, and the results are presented in Section 3. Finally, we conclude the paper in Section 4.

## 2. Materials and Methods

### 2.1. Synthesis

The precursors of NaBaInO<sub>4</sub> and Ca-doped NaBaInO<sub>4</sub> compounds were synthesized via solid-state reactions. For the NaBaInO<sub>4</sub>, the constituent component oxides, Nd<sub>2</sub>O<sub>3</sub> (Alfa Aesar, 99.9% purity), In<sub>2</sub>O<sub>3</sub> (Alfa Aesar, 99.9% purity), and BaCO<sub>3</sub> (Aldrich, 99+% purity) were accurately weighed in 1:1:1 cation molar ratios. As for Nd<sub>1-x</sub>Ca<sub>x</sub>BaInO<sub>4-x/2</sub> ( $x = 0.1, 0.2$ ), Nd<sub>2</sub>O<sub>3</sub>, CaCO<sub>3</sub> (AnalaR, 99.9% purity), BaCO<sub>3</sub>, and In<sub>2</sub>O<sub>3</sub> were exactly weighed in  $1 - x$ : $x$ :1:1 cation molar ratios. Then, the starting materials were mixed and finely ground using a ball mill for 3 h. Then, a controlled amount of dried mixed powder (about 1 g) was loaded into a polished cylindrical die cavity 13 mm in diameter and uniaxially prepressed into compacts through a rigid punch at 1.6 tonnes of weight for 2 min. In order to further enhance the density of the green compacts, a Stansted Fluid Power Isostatic Press (Model FPG2560A) was used to press them to 300 MPa pressure for 2 min.

The green pellets were first calcined at 1000 °C for 14 h. Then, undoped green pellets were sintered at 1440 °C; while green pellets, which were doped with 0.1 and 0.2 molar fractions of Ca<sup>2+</sup>, were sintered at 1430 °C and 1420 °C, respectively. The dwelling time for the sintering process was 20 h. The heating rate was 10 °C min<sup>-1</sup> for calcinations, while it was 20 °C min<sup>-1</sup> for the sintering progress. The cooling rate was 10 °C min<sup>-1</sup>.

### 2.2. Characterization of the Chemical Composition

The ceramic pellets were analysed via X-ray diffraction at room temperature to confirm the crystallographic data of the pellets. The incident X-rays scan the crystalline sample over a range of 2 $\theta$  angles as the same with the detector, which records the diffracted X-ray signals and counts signals. X-ray diffraction patterns were collected on an instrument called a Bruker D2 Phaser Diffractometer, which uses Cu-K $\alpha$  radiation ( $\lambda = 1.5418 \text{ \AA}$ ). Scans were continuous from 10° to 80° (2 $\theta$ ) with an increment of 0.032° (2 $\theta$ ) and step time of 0.9 s over a period of about 35 min. The analysis of crystallographic data was further performed with the Le Bail refinement by using the Fullprof refinement program and WinPLOTR software 2006 was used to plot the diffraction patterns.

### 2.3. Scanning Electron Microscopy and Energy Dispersive Spectrometry

In order to determine the optimum ball milling time, the morphologies of the starting ceramic powders, which were ball-milled for different lengths of time, were studied using an JEOL JSM-6010 LA analytical scanning electron microscope (JEOL, Tokyo, Japan) (using 20 kV with the working distance of 15 mm and 19 mm). The sample was coated with gold

via plasma sputtering at a sputtering current of 20 mA for 2 min. The instrument used for sputtering was a K550 Gold Target.

In addition, in order to analyse the porosity of pellets, the morphologies of the pellets' surface were characterized via scanning electron microscopy. Before characterization, these pellets were gradually ground using silicon carbide paper from 800-grit size to 4000-grit size. Then, all ceramic pellets were coated with gold using a sputter coater at a sputtering current of 20 mA for 2 min. The accelerating voltage used was 20 kV.

Furthermore, the cationic ratio of NaBaInO<sub>4</sub> and Ca-doped NaBaInO<sub>4</sub> compounds were confirmed via energy dispersive spectrometry (EDS).

#### 2.4. Electrical Conductivity Measurements

The electrical conductivities of NaBaInO<sub>4</sub> and Ca-doped NaBaInO<sub>4</sub> were first measured in the dry air, using a pellet sample via the standard 2-probe AC impedance spectroscopy method. A Solartron 1260 frequency response analyser (FRA) was employed, which used platinum mesh to form a contact. The tasks for the impedance measurements were set up using SMaRT (Version 3.2.1) software and the measurements ran automatically once the projects were created.

These sintered pellets were coated with electrode paste made of platinum and then cured at 800 °C for 1 h. The pellets were then annealed at 823 °C for 5 h before the impedance measurements, which were performed in the process of lowering the temperature from 760 °C to 270 °C at 50 °C intervals and the frequency range from 10<sup>7</sup> Hz to 1 Hz. The compressed air, which was dried using 98% sulfuric acid, was passed through the pipe to create a dry atmosphere.

Moreover, in order to investigate the effects of the humidified atmosphere on oxygen transport, the electrical conductivity measurements were also conducted in the wet atmosphere for NaBaInO<sub>4</sub> and Nd<sub>0.9</sub>Ca<sub>0.1</sub>BaInO<sub>3.95</sub> pellets separately using AC impedance spectroscopy. The pellets were also annealed at 823 °C for 5 h and measured in the same temperature range and frequency range as before. The wet atmosphere was created by making the compressed air flowing through a water bubbler at room temperature, and the humidity was estimated to be 2% (vol).

#### 2.5. Oxygen Isotope Exchange

Two samples composed of Nd<sub>0.9</sub>Ca<sub>0.1</sub>BaInO<sub>3.95</sub> and Nd<sub>0.8</sub>Ca<sub>0.2</sub>BaInO<sub>3.90</sub>, which have a relative density 97% of the calculated density, were chosen for the isotope exchange. Because the rough surface had diffusion entering from other directions, which affects the diffusion profile significantly, the samples were gradually ground using silicon carbide paper from 800-grit size to 4000-grit size and then polished down to 1 micron using polishing discs. Then, these well-polished surfaces were coated with a very thin layer of diluted platinum paste and curing was carried out at 800 °C for one hour in order to assist the isotope exchange.

After that, both samples were put into a tube and located next to a thermocouple. Before annealing, the tube was evacuated to a pressure of  $4 \times 10^{-7}$  mbar. Then, <sup>16</sup>O<sub>2</sub> with high purity (99.999%) was pumped into the tube to a pressure of 200 mbar and the two samples were both pre-annealed at 850 °C in a furnace under this atmosphere for 40 h, which is 10 times longer than that of <sup>18</sup>O<sub>2</sub> isotope exchange [14]. This pre-annealing process aims to remove the surface damage caused by polishing [15]. After these two samples were cooled down to room temperature, evacuation was performed again, as before, and 51.4% <sup>18</sup>O<sub>2</sub> was pumped into the tube to the same pressure. Then, the isotope exchange was performed at 850 °C for 4 h. At the end of the experiment, the <sup>18</sup>O<sub>2</sub> was recycled by liquid nitrogen due to the high cost of <sup>18</sup>O<sub>2</sub>.

#### 2.6. Secondary Ion Mass Spectrometry

Both samples were then cut perpendicular to the polished surface using the diamond saw and the cross sections of the samples were polished down to 1 micron with the same

steps as before. After preparation, the cross sections of both samples were analysed via SIMS with line scanning mode. The instrument was equipped with a Bi primary ion beam as well as a Cs secondary ion. The surface of the samples was cleaned by sputtering with 1 keV Cs until the yield of the contamination species had dropped to its minimum and the yield for  $^{16}\text{O}$  stopped changing. Then, the elements were detected using TOF mass spectroscopy.

### 3. Results and Discussion

#### 3.1. Ball Milling Time Determination

The secondary electron images of these ball-milled powders with different time intervals are shown in Figure 1. From the SEM micrographs, it is observed that the particle size becomes smaller and has more uniform distribution when the ball-milling time is increased to 3 h. The morphologies varied from irregular-shaped (1 h), to long and thick needle-shaped (2 h), and to short and thin needle-shaped (3 h) particles. When the ball-milling time increases to 4 h, the size of the needle-shaped particles become larger again. With further increases in the ball-milling time, the particles started to agglomerate, which has bad effects on the following sintering process; for instance, the porosity of the pellets will be increased. Finally, the size of a part of the particles becomes very large. As a result, 3 h milled powders are the optimum choice for the next sintering stage.

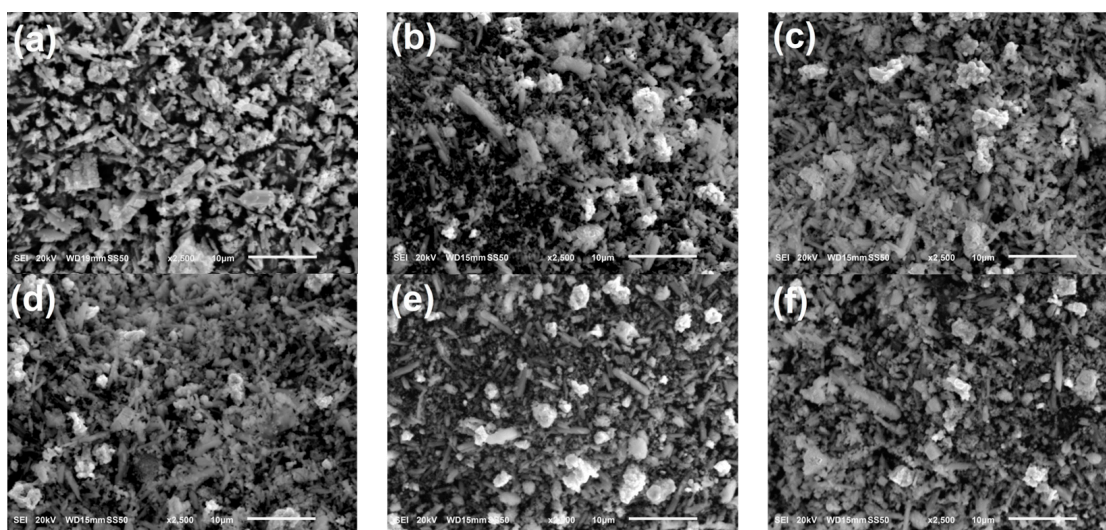


**Figure 1.** SEM micrographs of mixed powder ( $\text{Nd}_2\text{O}_3$ ,  $\text{BaCO}_3$  and  $\text{In}_2\text{O}_3$ ), which were ball-milled for (a) 1 h; (b) 2 h; (c) 3 h; (d) 4 h; (e) 5 h; and (f) 6 h.

#### 3.2. Crystal Structure of $\text{NaBaInO}_4$ and Ca-Doped $\text{NaBaInO}_4$ via Le Bail Refinement

The X-ray diffraction patterns of  $\text{NaBaInO}_4$  and Ca-doped  $\text{NaBaInO}_4$  compounds are shown in Figure 2. For  $\text{NaBaInO}_4$  compound, the experimental pattern shows no difference from the pattern that was reported by Fujii et al. [11]. Therefore, the sample can be confirmed to be  $\text{NdBaInO}_4$  compounds and no secondary phase was detected. In addition, the space group can be identified as  $\text{P}2_1/c$  and the structure system was confirmed to be monoclinic. Based on the X-ray diffraction data, which were detected using a Bruker D2 Phaser Diffractometer, Le Bail refinement was carried out for  $\text{NdBaInO}_4$ ,  $\text{Nd}_{0.9}\text{Ca}_{0.1}\text{BaInO}_{3.95}$ , and  $\text{Nd}_{0.8}\text{Ca}_{0.2}\text{BaInO}_{3.90}$  so as to explore the structure and crystal lattice parameters' changes in  $\text{NdBaInO}_4$  via 10 mol% and 20 mol% Ca doping. The final Le Bail patterns are shown in Figure 2 and the final refined crystallographic parameters are shown in Table 1.

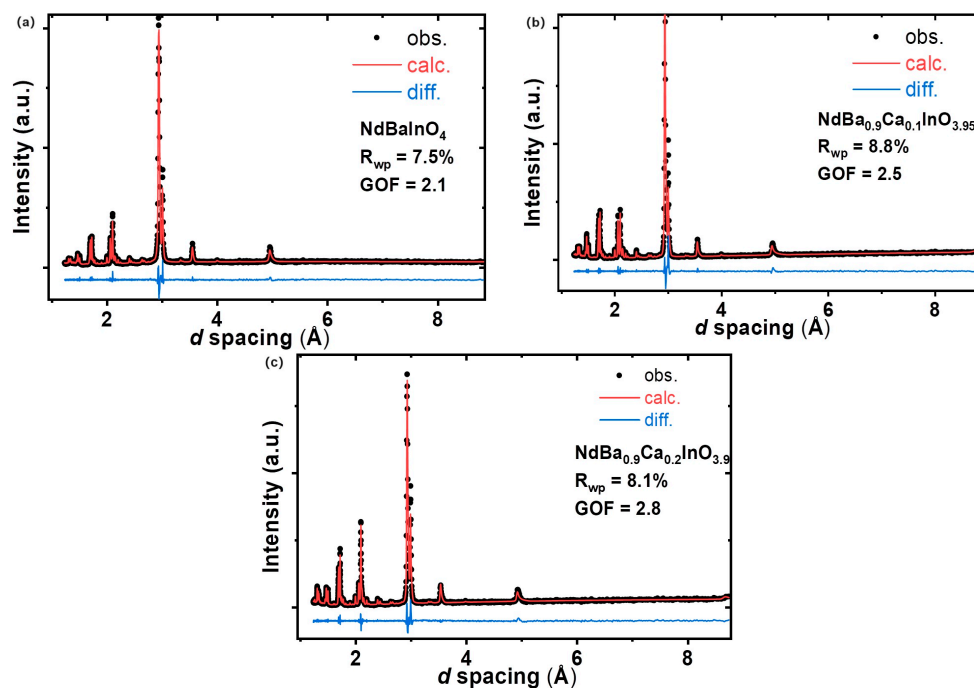


**Figure 2.** Le Bail refinement for the X-ray diffraction pattern collected at room temperature of (a)  $\text{NaBaInO}_4$ ; (b)  $\text{Nd}_{0.9}\text{Ca}_{0.1}\text{BaInO}_{3.95}$ ; and (c)  $\text{Nd}_{0.8}\text{Ca}_{0.2}\text{BaInO}_{3.90}$ . The experimental data are in black dots, the refined pattern is the red solid line, and the difference between the experimental and calculated data is the blue solid line.

**Table 1.** Crystallographic data of  $\text{NdBaInO}_4$  compared with data in the literature, and crystallographic data of  $\text{Nd}_{0.9}\text{Ca}_{0.1}\text{BaInO}_{3.95}$  and  $\text{Nd}_{0.8}\text{Ca}_{0.2}\text{BaInO}_{3.90}$  compared with data of  $\text{NdBaInO}_4$  resulting from experiment.

Chemical Formula	$\text{NdBaInO}_4$ Ref [11]	$\text{NdBaInO}_4$ Exp.	$\text{Nd}_{0.9}\text{Ca}_{0.1}\text{BaInO}_{3.95}$	$\text{Nd}_{0.8}\text{Ca}_{0.2}\text{BaInO}_{3.90}$
Formula weight	460.39	460.39	449.17	437.96
Crystal system	Monoclinic	Monoclinic	Monoclinic	Monoclinic
Space group	$P2_1/c$	$P2_1/c$	$P2_1/c$	$P2_1/c$
$a/\text{Å}$	9.09538(3)	9.1079(16)	9.0926(10)	9.0822(17)
$b/\text{Å}$	6.04934(2)	6.0522(11)	6.0322(9)	6.0195(12)
$c/\text{Å}$	8.25620(2)	8.2815(14)	8.2636(10)	8.2613(14)
$\beta/^\circ$	103.4041(3)	103.486(13)	103.392 (9)	103.337(19)
Unit-cell volume/ $\text{Å}^3$	441.89(2)	443.92(14)	440.92(10)	439.47(15)
Calculated density/ $\text{Mg m}^{-3}$	6.92		6.78	6.63
Measured density/ $\text{Mg m}^{-3}$		6.68	6.55	6.45
Relative density		96.53%	96.61%	97.29%

As for Ca-doped  $\text{NaBaInO}_4$  compounds, their experimental patterns (peak positions and peak shapes) are in great agreement with Le Bail refinement patterns. Therefore, the refined lattice parameters can be determined accurately and the results are also shown in Table 1. In addition, there is no other peak appearing when compared with the experimental patterns of  $\text{NaBaInO}_4$  compounds. As a result,  $\text{Nd}_{0.9}\text{Ca}_{0.1}\text{BaInO}_{3.95}$  and  $\text{Nd}_{0.8}\text{Ca}_{0.2}\text{BaInO}_{3.90}$  can also be identified as being of the monoclinic  $P2_1/c$   $\text{NaBaInO}_4$  phase.

### 3.3. Fractional Change in Crystallographic Data

The variations in crystal lattice parameters between  $\text{NdBaInO}_4$  and 10 mol% and 20 mol% Ca-doped  $\text{NdBaInO}_4$  were investigated in this work. The fractional changes in lattice parameters ( $a$ -,  $b$ - and  $c$ -axes;  $\beta$ -angle; and unit-cell volume  $V$ ) compared with  $\text{NdBaInO}_4$  are shown in Figure 3. It is observed that apart from  $c$ -axes, which are slightly

increased, and the  $\beta$ -angle, which is stable, other unit-cell parameters and the unit-cell volume drop significantly when the molar fraction of Ca-doping is raised to 0.2. The inconsistent trend for c-axes values compared with others can be attributed to the big step size set during the X-ray diffraction analysis. A big step size gives rise to a short data collection time and, thus, insufficient data, which influence the accuracy of Le Bail refinement.

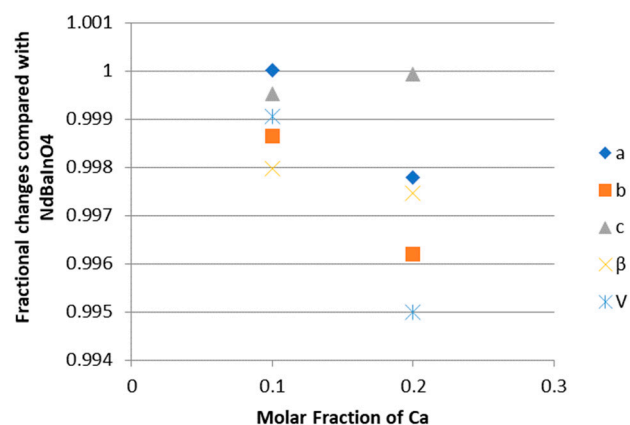


**Figure 3.** Fractional changes in lattice parameters (a-, b-, and c-axes;  $\beta$ -angle; and unit-cell volume V) of 10 mol% and 20 mol% Ca-doped NdBaInO<sub>4</sub> compared with undoped NdBaInO<sub>4</sub>.

This phenomenon can be interpreted in terms of the effective ionic radii of the Ca<sup>2+</sup> dopant and in other respects such as defects. The effective ionic radius of Nd<sup>3+</sup> (CN=9) is 1.163 Å, which is a little smaller than that of Ca<sup>2+</sup> (CN=9) which is 1.18 Å. The ionic radii presented in this work are all taken from Shannon [16]. Therefore, it should have experience expansion of the unit-cell after doping. However, some defects such as oxygen vacancies will be introduced after doping, which indicates that the distances between the ions will be altered and, thus, deformation may occur. So, there must be some balance between the increase in ionic radii and introduction of oxygen vacancies. In this system, it is very likely that Ca<sup>2+</sup> with a bigger radius has interaction with oxygen vacancies and finally results in the reduction of the lattice parameters as well as the unit-cell volume. But, the specific interactions have not been studied and investigated in this paper and the further work need to be conducted to explain this phenomenon.

### 3.4. Microscope Structure of NaBaInO<sub>4</sub> and Ca-Doped NaBaInO<sub>4</sub>

The surface topography of an NdBaInO<sub>4</sub> pellet with a relative density of 93.7% of theoretical density was observed via SEM and the images are shown in Figure 4. The pictures with low magnification show that there are a lot of obvious pores; the majority of them are closed pores and a few pores are connected to each other, which demonstrates it is a pellet with high density. From the images taken in high magnification ( $\times 2500$ ), the size of some small pores is estimated to be 1–2 microns, while the size of some large pores are 5 microns or bigger.

The surface topography of the pellets composed of Nd<sub>0.9</sub>Ca<sub>0.1</sub>BaInO<sub>3.95</sub> and Nd<sub>0.8</sub>Ca<sub>0.2</sub>BaInO<sub>3.90</sub> with the relative density of 96.6% and 97.3% of calculated density, respectively, was also observed via SEM and the images are shown in Figure 5. There are some scratches on the surface due to rough polishing with the silicon carbide papers. Apart from some obvious pores, which are in black colour and round in shape, some craters with some particles attached on the surface can be seen from the first two images in particular. This unexpected surface topography may result from the incomplete and rough polishing and contaminants produced during polishing.

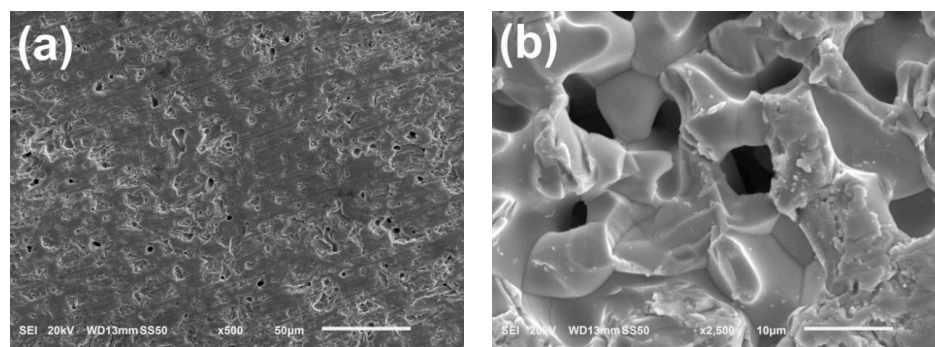


**Figure 4.** Secondary electron images of the polished surface of a  $\text{NaBaInO}_4$  pellet with 93% density: (a) 500 magnification; (b) 2500 magnification.

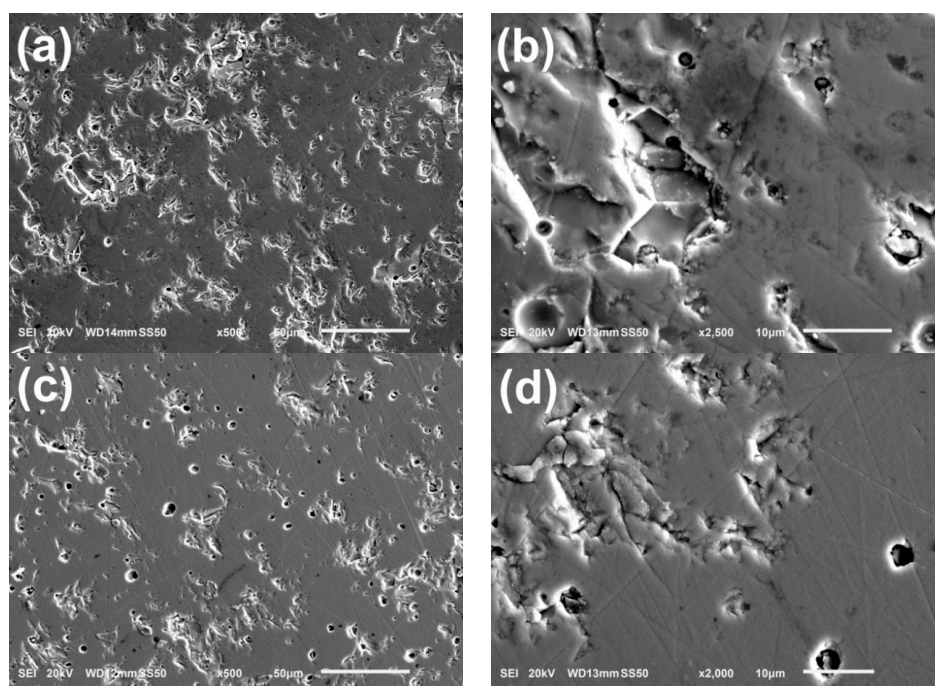


**Figure 5.** Secondary electron images of the polished surface of a  $\text{Nd}_{0.9}\text{Ca}_{0.1}\text{BaInO}_{3.95}$  pellet with 96.6% relative density with (a) 500 magnification and (b) 2500 magnification and a  $\text{Nd}_{0.8}\text{Ca}_{0.2}\text{BaInO}_{3.90}$  pellet with 97.3% relative density with (c) 500 magnification and (d) 2000 magnification.

### 3.5. Energy Dispersive Spectrometry

In order to deduce the stoichiometric ratio of synthesized materials quantitatively, energy-dispersive spectrometry analysis was applied in different surface areas of polished samples. The EDS spectra and quantitative stoichiometric values are shown in Figure 6 and Table 2, respectively. It is observed that, apart from Nd, Ba, In, Ca, and O signals, Au and C signals were also detected, which can be attributed to the Au thin film that was sputter coated on the surface before detection and some organic contaminants produced during sample preparation. It is noticeable that the cationic ratio of Nd, Ba, and In is quite close to 1:1:1 for  $\text{NaBaInO}_4$ . Due to inherent difficulties in the accurate detection of light elements such as oxygen via EDS, the values of O can be overlooked. In addition, it is important to bear in mind the errors associated with using default remote standards pre-loaded into the analysis software—the results can be described as semi-quantitative at best. Therefore, the key result of EDS analysis is that no unexplainable elements were detected, which supports the XRD results.

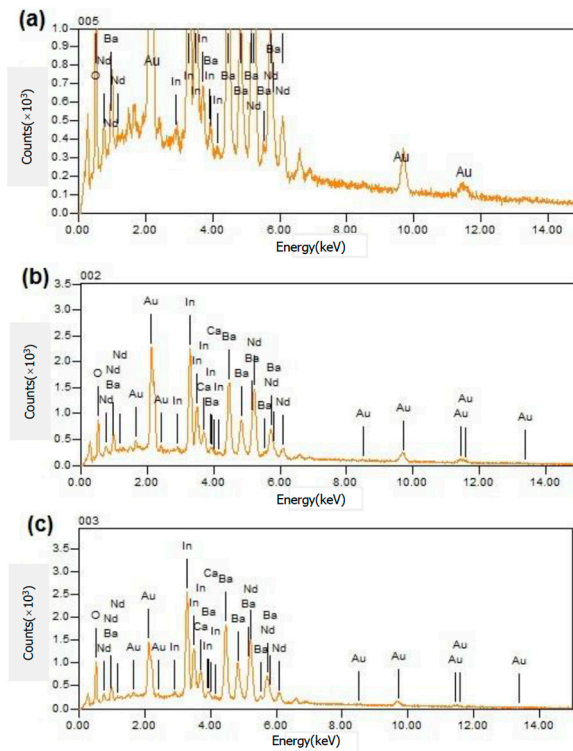


**Figure 6.** Energy dispersive spectra detected from a polished surface of (a)  $\text{NaBaInO}_4$ ; (b)  $\text{Nd}_{0.9}\text{Ca}_{0.1}\text{BaInO}_{3.95}$ ; and (c)  $\text{Nd}_{0.8}\text{Ca}_{0.2}\text{BaInO}_{3.90}$ .

**Table 2.** The atomic ratio of  $\text{NaBaInO}_4$  and Ca-doped  $\text{NaBaInO}_4$  compounds, which were detected via energy dispersive spectrometry (EDS).

	$\text{NaBaInO}_4$	$\text{Nd}_{0.9}\text{Ca}_{0.1}\text{BaInO}_{3.95}$	$\text{Nd}_{0.8}\text{Ca}_{0.2}\text{BaInO}_{3.90}$
<b>Elements</b>			
In, atom%	14.21	15.81	14.68
Ba, atom%	12.53	16.28	15.34
Nd, atom%	15.20	14.93	12.91
Ca, atom%		1.54	2.29

### 3.6. Temperature Programme Modification

In this work, the temperature programme of heat treatment was improved and modified in order to achieve higher densities of pellets. The theoretical density reported by Fujii et al. is  $6.92 \text{ Mg m}^{-3}$  and relative densities obtained in this work are based on it. When the sintering time was reduced from 24 h to 22 h at  $1400 \text{ }^\circ\text{C}$  sintering temperature, the density was enhanced. In this work,  $1450 \text{ }^\circ\text{C}$  sintering temperature was first tried for  $\text{NdBaInO}_4$  and the sintering time was reduced to 20 h. But, the pellets were found to be molten and evaporated away at the end of heat treatment. Therefore, the sintering temperature for  $\text{NdBaInO}_4$  was increased from  $1410 \text{ }^\circ\text{C}$  to  $1440 \text{ }^\circ\text{C}$ . By increasing the temperature, the relative density was improved from about 92% to more than 96%.

Generally, doping the materials with other elements will reduce the melting point. As a result, sintering temperatures for  $\text{Nd}_{0.9}\text{Ca}_{0.1}\text{BaInO}_{3.95}$  and  $\text{Nd}_{0.8}\text{Ca}_{0.2}\text{BaInO}_{3.90}$  were set to be  $1430 \text{ }^\circ\text{C}$  and  $1420 \text{ }^\circ\text{C}$ , respectively. Because there is no theoretical density that can be referenced for Ca-doped  $\text{NdBaInO}_4$ , the density calculated with refined lattice parameters was used as the theoretical density. The results show that the relative density could even achieve 97% after modifications.

### 3.7. Electrical Conductivity of NdBaInO<sub>4</sub> and Ca-Doped NdBaInO<sub>4</sub> in Dry Air

The electrical conductivities of NdBaInO<sub>4</sub> were measured in dry air and the Nyquist plots of its impedance data at low temperature (280 °C) and high temperature (720 °C) are shown in Figure 7a,b. The AC impedance data of NdBaInO<sub>4</sub> at low temperature were perfectly fitted with two equivalent circuits, which are both composed of R-CPE elements. However, there is only one semicircle, which is observable in Figure 7a; this means the semicircle that corresponds to the bulk component overlaps with the semicircle that corresponds to the grain boundary component. Therefore, the total resistance of NdBaInO<sub>4</sub> at 280 °C can be calculated as the sum of the resistance of the bulk and grain boundary or can be obtained from the right intercept of the semicircle and the resulting value is  $9.9 \times 10^5 \Omega$ . However, the resistance of the rig (about 4  $\Omega$ ) also exists in the system, so it is necessary to remove the contribution of the rig resistance to obtain the actual resistance of the sample. It is so small when compared with the total resistance at low temperature, but it has a significant contribution to the total resistance when the temperature goes higher.

At high temperature, the bulk response is absent due to the instrumental detection limit, so it is difficult to fit the whole impedance data. For the high frequency response, the shape of the semicircle is no longer observed; hence, only the low frequency response was fitted and the capacitance was estimated to be  $4.4 \times 10^{-10}$  F. In order to assign the corresponding semicircles to the different regions of the sample, it is multiplied by  $l/A = 0.149 \text{ cm}^{-1}$  of the pellet, giving the result of  $6.56 \times 10^{-11}$  F. Therefore, this low frequency response corresponds to the grain boundary component and the total resistance of the sample can be obtained from the right intercepts of the semicircle. The resulting resistance is 3480  $\Omega$ , after being reduced by 4  $\Omega$  of the rig resistance.

The electrical conductivities of Nd<sub>0.9</sub>Ca<sub>0.1</sub>BaInO<sub>3.95</sub> and Nd<sub>0.8</sub>Ca<sub>0.2</sub>BaInO<sub>3.90</sub> in the dry air were also measured and the Nyquist plots of their impedance data at low temperatures and high temperatures are shown in Figure 7c–f. As for Nd<sub>0.9</sub>Ca<sub>0.1</sub>BaInO<sub>3.95</sub> at low temperature (270 °C), from Figure 7c and the enlarged view in it, it is obviously observed that there are three frequency responses and the grain boundary region, which corresponds to the middle frequency response, is significantly overlapped with the sample–electrode interface region. But, it is difficult to use the R-CPE elements to fit them; hence, only the sample–electrode interface region was fitted manually and the total resistance of the sample at low temperature can be estimated to be the left intercept of the sample–electrode interface semicircle on the  $Z'$  axis, giving the result of 39,585  $\Omega$ . Compared with the impedance spectra at low temperature, it can be deduced that the semicircle in the middle of the high temperature impedance spectra corresponds to the sample–electrode interface component. As can be seen from the Figure 7d, a part of the sample–electrode interface semicircle is in the positive imaginary impedance area; as a consequence, the intersection of this semicircle and  $Z'$  axis can be directly regarded as the total resistance of the pellet at high temperature. Then, after being reduced by 4  $\Omega$  of the rig resistance, the resulting value of Nd<sub>0.9</sub>Ca<sub>0.1</sub>BaInO<sub>3.95</sub> was calculated to be 33.4  $\Omega$  for the dry atmosphere.

As for Nd<sub>0.8</sub>Ca<sub>0.2</sub>BaInO<sub>3.90</sub> at low temperature (390 °C) in Figure 7e, it can be obviously seen that there are two complete semicircles, which correspond two frequency responses. After being multiplied by  $l/A = 0.196 \text{ cm}^{-1}$ , the capacitance of the low frequency response was estimated to be  $3.45 \times 10^{-9}$  F, which can be assigned to the grain boundary component. Then, these two semicircles were perfectly fitted with two equivalent circuits, which are both composed of R-CPE elements, and the corresponding resistances for the bulk and grain boundary were fitted to be 4469  $\Omega$  and 28,981  $\Omega$ , respectively. Therefore, the total electrical resistance of Nd<sub>0.8</sub>Ca<sub>0.2</sub>BaInO<sub>3.90</sub> at low temperature was calculated to be 33,450  $\Omega$ . At high temperature (760 °C), the high frequency response is in the positive imaginary impedance area and the total resistance can be directly calculated to be the right intercept of the grain boundary semicircle (low frequency) on the  $Z'$  axis, giving the result of 47.2  $\Omega$ . The same methodology was used to fit all of the data set.

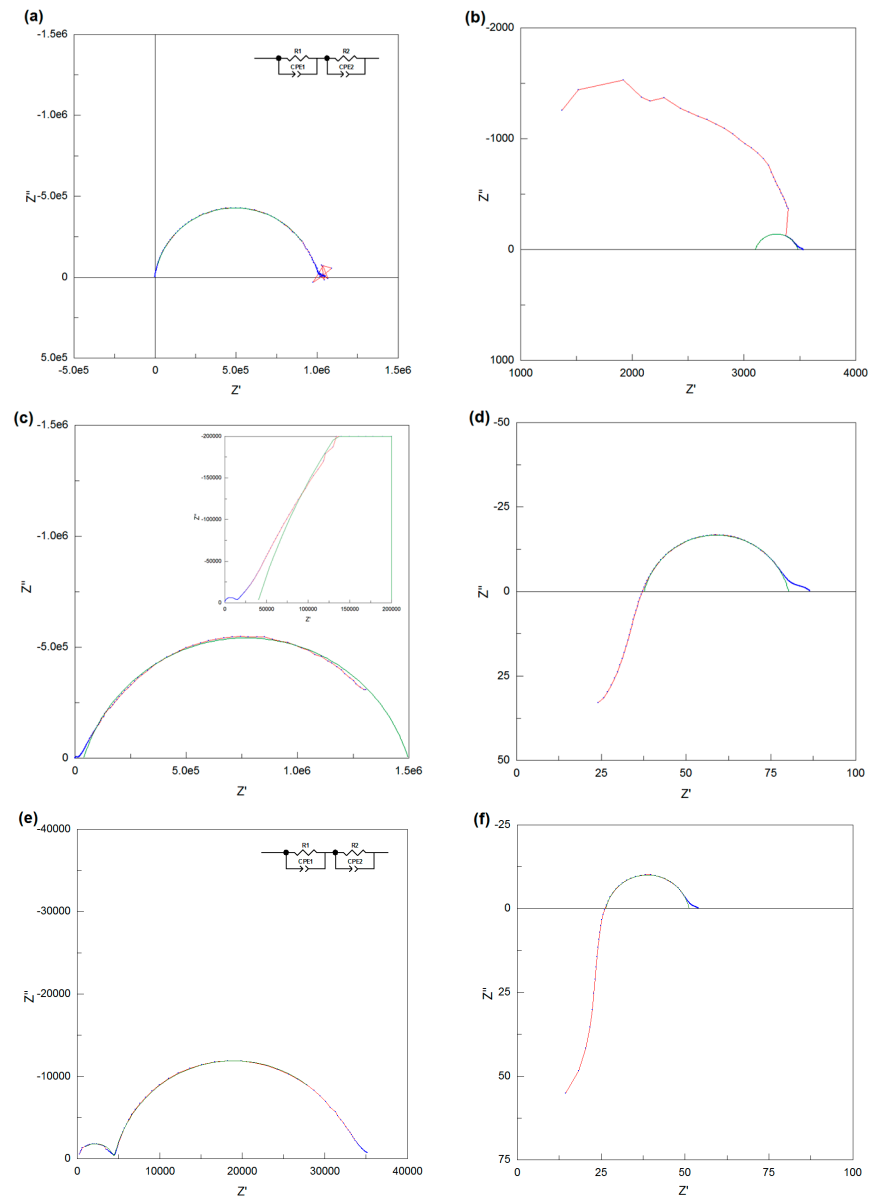


**Figure 7.** Impedance spectra measured in the dry air at (a) 280 °C and (b) 720 °C for NdBaInO<sub>4</sub>; (c) 270 °C and (d) 760 °C for Nd<sub>0.9</sub>Ca<sub>0.1</sub>BaInO<sub>3.95</sub>; and (e) 390 °C and (f) 760 °C for Nd<sub>0.8</sub>Ca<sub>0.2</sub>BaInO<sub>3.90</sub>. The experimental data are in red solid lines with blue dots; the fitting curves are in green solid lines. The equivalent circuits used in (a,e) to model each physical feature are inserted in the spectra.

The total resistance, which was determined via impedance spectroscopy data, can be transformed into the total conductivity using Equation (1):

$$\sigma = \frac{l}{AR} \tag{1}$$

where  $\sigma$  is the total conductivity (S m<sup>-1</sup>),  $l$  is the thickness of the pellet (m),  $A$  is the surface area of the pellet (cm<sup>2</sup>), and  $R$  is the total resistance ( $\Omega$ ).

The total conductivity is expressed by the Arrhenius equation [17] (Equation (2)):

$$\sigma = \frac{\sigma_0}{T} \exp\left(\frac{-E_a}{RT}\right) \tag{2}$$

where  $E_a$  is the activation energy ( $\text{J mol}^{-1}$ ),  $R$  is the gas constant ( $\text{J K}^{-1} \text{mol}^{-1}$ ),  $T$  is the temperature (K), and  $\sigma_0$  is a pre-exponential factor.

Therefore, the logarithm of conductivity against the reciprocal of temperature is commonly plotted to obtain a linear relationship. The results of  $\text{NdBaInO}_4$  and Ca-doped  $\text{NdBaInO}_4$ , which were measured in dry air, are shown in Figure 8 and Table 3.

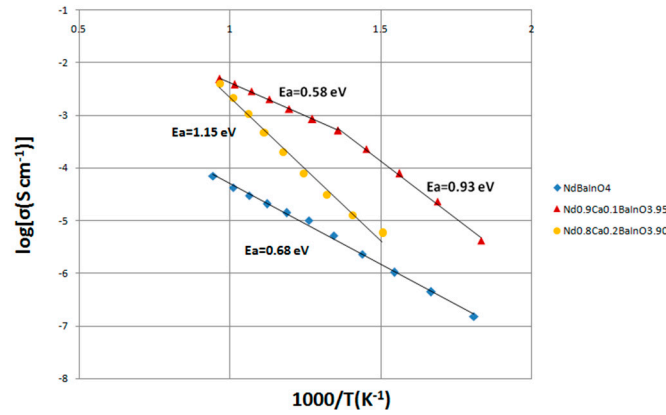


**Figure 8.** The Arrhenius plot of the total conductivity of  $\text{NdBaInO}_4$  and Ca-doped  $\text{NdBaInO}_4$  measured in dry air.

**Table 3.** Electrical conductivity of  $\text{NdBaInO}_4$  and Ca-doped  $\text{NdBaInO}_4$  in dry air.

	$\text{NdBaInO}_4$	$\text{Nd}_{0.9}\text{Ca}_{0.1}\text{BaInO}_{3.95}$	$\text{Nd}_{0.8}\text{Ca}_{0.2}\text{BaInO}_{3.90}$
R at low temperature ( $\Omega$ )	$9.9 \times 10^5$ (at 280 °C)	39,585 (at 270 °C)	33,450 (at 390 °C)
R at high temperature ( $\Omega$ )	3480 (at 720 °C)	33.4 (at 760 °C)	47.2 (at 760 °C)
$\sigma$ ( $\text{S cm}^{-1}$ )	$6.36 \times 10^{-5}$ (at 760 °C)	$4.91 \times 10^{-3}$ (at 760 °C)	$4.14 \times 10^{-3}$ (at 760 °C)
$E_a$ (eV)	0.68	0.93 (below 464 °C) 0.58 (above 464 °C)	1.15

From the Arrhenius equation, it is obvious that low activation energy has the benefit of promoting total electrical conductivity. Therefore, it is important to determine the activation energy; in order to obtain its value, the Arrhenius equation can be rearranged to Equation (3) by taking the natural logarithm:

$$\ln(\sigma T) = -\frac{E_a}{RT} + \ln(\sigma_0). \quad (3)$$

Then, a plot of the  $\ln(\sigma T)$  against the reciprocal of temperature gives a straight line and the activation energy ( $E_a$ ) can be calculated from the gradient of the line by multiplying the gas constant  $R$ , which is  $8.314 \text{ J K}^{-1} \text{ mol}^{-1}$ , giving the results of 0.68 eV for  $\text{NdBaInO}_4$ . It can be seen from Figure 8 that the total electrical conductivity of  $\text{NdBaInO}_4$  at 760 °C in the dry atmosphere is about  $6.36 \times 10^{-5} \text{ S cm}^{-1}$ . In addition, the activation energy  $E_a$  of  $\text{Nd}_{0.9}\text{Ca}_{0.1}\text{BaInO}_{3.95}$  (0.93 eV) is relatively higher than that of  $\text{NdBaInO}_4$  (0.68 eV) when the temperature is below 464 °C. The possible explanation for this phenomenon is that at low temperatures the dopant aliovalent cations can be seen as the nucleation centres where oxygen vacancies and dopant cations bind together into defect clusters with low mobility. When the temperature is above 464 °C (737 K), those bound vacancies are dissolved and become mobile, which reduces the activation energy  $E_a$  to 0.58 eV, which is lower than that of  $\text{NdBaInO}_4$ , indicating better mobility of the oxygen species in  $\text{Nd}_{0.9}\text{Ca}_{0.1}\text{BaInO}_{3.95}$ . Moreover, after doping the  $\text{NdBaInO}_4$  with a 10% molar fraction of  $\text{Ca}^{2+}$ , it can be seen from the Figure 8 that the total electrical conductivity of the sample at 760 °C has been significantly increased by two orders of magnitude ( $4.91 \times 10^{-3} \text{ S cm}^{-1}$ ) due to the generation of oxygen vacancies.

When the Ca dopant concentration was increased to a 20% molar fraction, the activation energy was raised to 1.15 eV, which is even bigger than that of the  $\text{NdBaInO}_4$ , but the total electrical conductivity was improved to a certain extent when compared with the undoped material. Above all,  $\text{Nd}_{0.9}\text{Ca}_{0.1}\text{BaInO}_{3.95}$  exhibited the highest total electrical conductivity and the lowest activation energy among  $\text{Nd}_{1-x}\text{Ca}_x\text{BaInO}_{4-x/2}$  ( $x = 0, 0.1$  and  $0.2$ ).

### 3.8. The Effects of the Humidified Atmosphere on the Conductivity of $\text{NdBaInO}_4$ and $\text{Nd}_{0.9}\text{Ca}_{0.1}\text{BaInO}_{3.95}$

The electrical conductivity measurements were also conducted in the wet atmosphere for  $\text{NdBaInO}_4$  and  $\text{Nd}_{0.9}\text{Ca}_{0.1}\text{BaInO}_{3.95}$  pellets separately using AC impedance spectroscopy; the Nyquist plots of the impedance data for  $\text{Nd}_{0.9}\text{Ca}_{0.1}\text{BaInO}_{3.95}$  at low temperature ( $270\text{ }^\circ\text{C}$ ) and high temperature ( $760\text{ }^\circ\text{C}$ ) in the wet atmosphere are shown in Figure 9. As with the Nyquist plots of the dry atmosphere, the sample–electrode interface region was fitted manually and the total resistance of the sample at low temperature can be estimated to be the left intercept of the sample–electrode interface semicircle on the  $Z'$  axis, giving the result of  $9089.4\ \Omega$ . At high temperature, the intersection of the semicircle and  $Z'$  axis can be directly regarded as the total resistance of the pellet. Then, after being reduced by  $4\ \Omega$  of the rig resistance, the resulting value of  $\text{Nd}_{0.9}\text{Ca}_{0.1}\text{BaInO}_{3.95}$  was calculated to be  $31.7\ \Omega$  for the wet atmosphere.

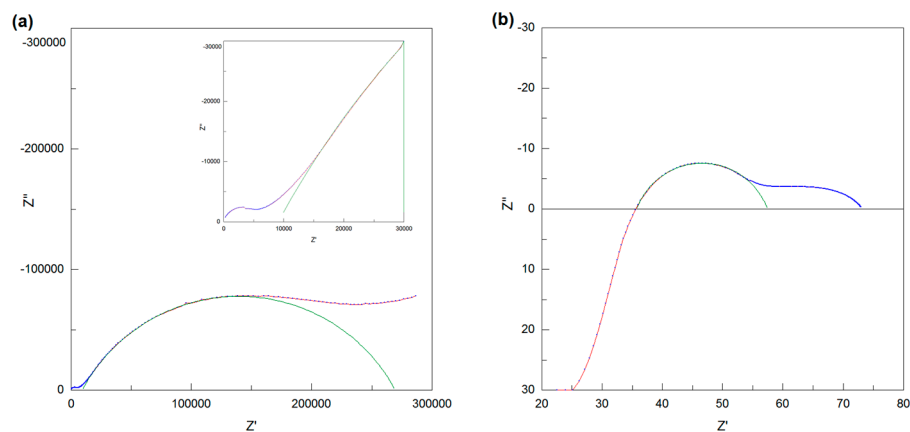


**Figure 9.** Impedance spectra of  $\text{Nd}_{0.9}\text{Ca}_{0.1}\text{BaInO}_{3.95}$  measured in the wet atmosphere at (a) low temperature ( $270\text{ }^\circ\text{C}$ ) and (b) high temperature ( $760\text{ }^\circ\text{C}$ ). The experimental data are in red solid lines with blue dots; the fitting curves are in green solid lines.

As before, the logarithm of the total conductivity against the inverse temperature of undoped and 10% Ca-doped material were also plotted to obtain linear relationships and the resulting graph is displayed in Figure 10. It can be observed that the total conductivity of  $\text{Nd}_{0.9}\text{Ca}_{0.1}\text{BaInO}_{3.95}$  measured in the wet atmosphere at moderate temperature is relatively higher than that in the dry atmosphere. On the contrary, the total conductivity of the undoped pellet that was performed in the dry atmosphere is slightly higher than that in the wet atmosphere. So, this slight deviation at low temperature requires further investigation. Therefore, the excess conductivity of  $\text{Nd}_{0.9}\text{Ca}_{0.1}\text{BaInO}_{3.95}$  in the wet atmosphere suggests that potential proton conduction may exist because oxygen vacancies generally make contributions to proton conduction. Moreover, the proton conductivity of the doped material reaches the maximum and the total conductivity tends to be uniform at a certain high temperature ( $800\text{ }^\circ\text{C}$ ), which might result from the depleted proton charge carrier at elevated temperatures. Similar behaviour has been observed in other proton-conducting systems such as  $\text{BaCeZr}_{3-d}$  and Ca-doped  $\text{LaNbO}_4$  [18].

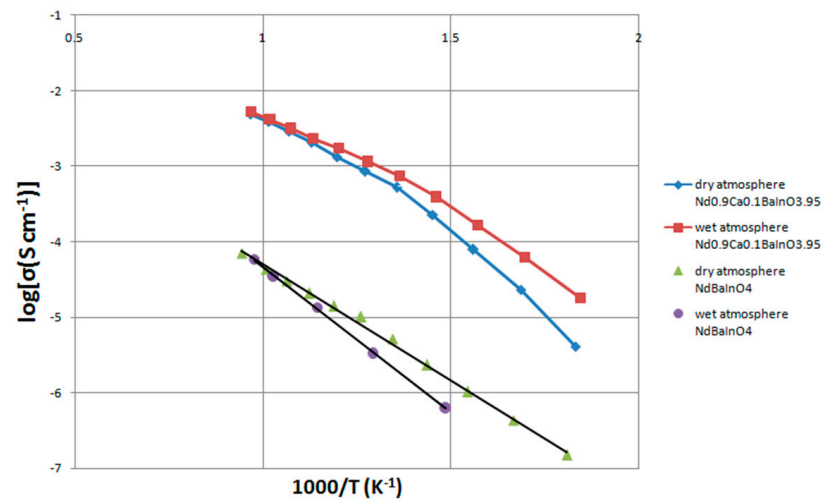


**Figure 10.** The Arrhenius plot of the total conductivities of  $\text{NdBaInO}_4$  and  $\text{Nd}_{0.9}\text{Ca}_{0.1}\text{BaInO}_{3.95}$  measured in the dry atmosphere and wet atmosphere.

### 3.9. IEDP of Ca-Doped $\text{NdBaInO}_4$

The diffusion profile was obtained via TOF-SIMS and one of the profiles for 20%-doped sample are shown in Figure 11. These experimental data were fitted appropriately using a MatLab R2013a script that utilized the least square fitting to obtain  $k^*$  and  $D^*$  parameters. The results of the diffusion coefficients and surface exchange coefficients are listed in Table 4 and the fitting error, which was introduced by the measurement, should be around 10% percent. The oxygen diffusion coefficients of  $\text{Nd}_{0.9}\text{Ca}_{0.1}\text{BaInO}_{3.95}$  ( $D^* = 1.82 \times 10^{-8} \text{ cm}^2/\text{s}$ ,  $850^\circ\text{C}$ ) is about two times higher than that of  $\text{Nd}_{0.8}\text{Ca}_{0.2}\text{BaInO}_{3.90}$  ( $D^* = 7.95 \times 10^{-9} \text{ cm}^2/\text{s}$ ,  $850^\circ\text{C}$ ). When compared with the oxygen diffusion coefficient of the undoped  $\text{NdBaInO}_4$  ( $D^* = 8.25 \times 10^{-11} \text{ cm}^2/\text{s}$ ,  $850^\circ\text{C}$ ), the diffusion coefficients of  $\text{Nd}_{0.9}\text{Ca}_{0.1}\text{BaInO}_{3.95}$  was increased significantly by two orders of magnitude. In addition, it is worth noting that  $\text{Nd}_{0.9}\text{Ca}_{0.1}\text{BaInO}_{3.95}$  shows the highest diffusion coefficient and  $D^*$  decreases with the increase in the molar fraction of the Ca element, since when the doping concentration exceeds certain value the ordered-vacancy phase will be formed, which leads to a dramatic drop in conductivity. As the surface of both samples was coated with a thin layer of Pt, the surface of them cannot be characterized by the obtained surface exchange coefficient.

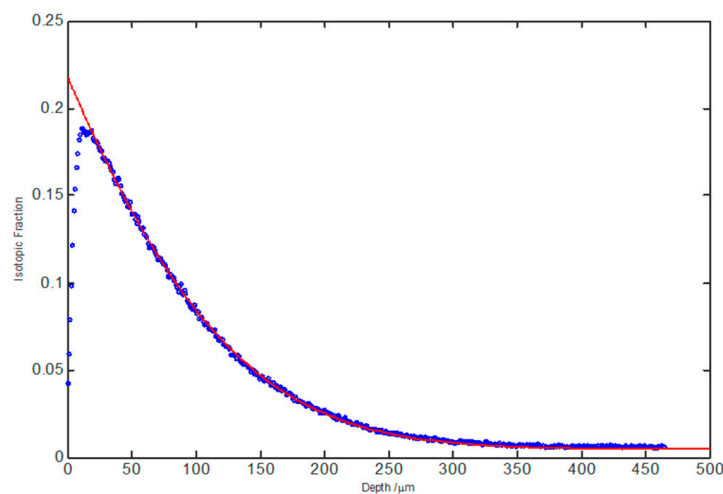


**Figure 11.** The fitting of the  $^{18}\text{O}$  line scanning diffusion profile for  $\text{Nd}_{0.8}\text{Ca}_{0.2}\text{BaInO}_{3.90}$ . Experimental data are in blue dots and the fitting result is the red solid line.

**Table 4.** Calculated oxygen diffusion coefficients and surface exchange coefficients of the samples doped with 10% and 20% molar fraction of Ca<sup>2+</sup>.

	Nd <sub>0.9</sub> Ca <sub>0.1</sub> BaInO <sub>3.95</sub>	Nd <sub>0.8</sub> Ca <sub>0.2</sub> BaInO <sub>3.90</sub>
D* (cm <sup>2</sup> /s)	1.82 × 10 <sup>-8</sup>	9.30 × 10 <sup>-9</sup>
Average D* (cm <sup>2</sup> /s)	1.80 × 10 <sup>-8</sup>	6.60 × 10 <sup>-9</sup>
k* cm.s <sup>-1</sup>	1.81 × 10 <sup>-8</sup>	7.95 × 10 <sup>-9</sup>
	6.60 × 10 <sup>-7</sup>	7.00 × 10 <sup>-7</sup>

#### 4. Conclusions

The synthesis method used in this work is the solid-state reaction and three-hour ball-milling has been determined to be the optimum choice for the next sintering stage. In addition, the temperature programme of heat treatment has been improved and modified in order to achieve higher densities. The sintering temperatures for NdBaInO<sub>4</sub>, Nd<sub>0.9</sub>Ca<sub>0.1</sub>BaInO<sub>3.95</sub>, and Nd<sub>0.8</sub>Ca<sub>0.2</sub>BaInO<sub>3.90</sub> have been increased from 1400 °C to 1440 °C and 1430 °C and 1420 °C, respectively, and the sintering time has been reduced from 24 h to 20 h. By increasing sintering temperatures and reducing the time, the relative densities were improved dramatically from about 92% to more than 96%.

The results of X-ray diffraction analysis indicate that NdBaInO<sub>4</sub> compounds with a single phase of monoclinic P2<sub>1</sub>/c were successfully synthesized and it remains as this single-phase structure after doping 0.1 and 0.2 molar fractions of Ca<sup>2+</sup> into the Nd site. Then, the lattice parameters were determined via Le Bail refinement of the XRD data. The results show that apart from c-axes, which are slightly increased, and β-angle, which is stable, other unit-cell parameters and the unit-cell volume drop significantly when the molar fraction of Ca-doping is raised to 0.2. Moreover, the stoichiometric ratios of these synthesized materials were further confirmed by energy dispersive spectrometry. The cationic ratio of Nd, Ba, and In is quite close to 1:1:1 for NdBaInO<sub>4</sub> and the detected Ca concentration is quite reasonable for Ca-doped NdBaInO<sub>4</sub>.

The total electrical conductivity of NdBaInO<sub>4</sub> at 760 °C in the dry atmosphere is about 6.36 × 10<sup>-5</sup> S cm<sup>-1</sup>. However, after doping the NdBaInO<sub>4</sub> with 0.1 molar fraction of Ca<sup>2+</sup>, the total electrical conductivity at 760 °C significantly increased by two orders of magnitude (4.91 × 10<sup>-3</sup> S cm<sup>-1</sup>) and the activation energy reduced from 0.68 eV to 0.58 eV when the temperature was above 464 °C (737 K). Moreover, after doping 0.1 molar fraction of Ca<sup>2+</sup>, the activation energy was raised to 0.93 eV when the temperature was below 464 °C (737 K), which is possible due to the formation of the defect clusters with low mobility. Although the activation energy of Nd<sub>0.8</sub>Ca<sub>0.2</sub>BaInO<sub>3.90</sub> (1.15 eV) is even larger than that of undoped material, the total conductivity was also improved. Above all, Nd<sub>0.9</sub>Ca<sub>0.1</sub>BaInO<sub>3.95</sub> exhibited the highest total electrical conductivity and the lowest activation energy among Nd<sub>1-x</sub>Ca<sub>x</sub>BaInO<sub>4-x/2</sub> (x = 0, 0.1 and 0.2).

In addition, the total conductivity of Nd<sub>0.9</sub>Ca<sub>0.1</sub>BaInO<sub>3.95</sub> in the wet atmosphere at moderate temperature is relatively higher than that in the dry atmosphere. Therefore, the excess conductivity suggests that potential proton conduction may exist in wet atmospheres. In addition, the proton conductivity reaches the maximum and the total conductivity tends to be uniform at a certain high temperature.

The oxygen diffusion coefficient of Nd<sub>0.9</sub>Ca<sub>0.1</sub>BaInO<sub>3.95</sub> (D\* = 1.82 × 10<sup>-8</sup> cm<sup>2</sup>/s, 850 °C) is about two times higher than that of Nd<sub>0.8</sub>Ca<sub>0.2</sub>BaInO<sub>3.90</sub> (D\* = 7.95 × 10<sup>-9</sup> cm<sup>2</sup>/s, 850 °C) and was increased significantly by two orders of magnitude when compared with the oxygen diffusion coefficient of the undoped NdBaInO<sub>4</sub> (D\* = 8.25 × 10<sup>-11</sup> cm<sup>2</sup>/s, 850 °C).

**Author Contributions:** Software, M.C.; validation, M.C. and C.L.; formal analysis, M.C. and C.L.; investigation, J.W. and S.L.; data curation, W.K. and Z.B.; writing—original draft preparation, M.C.; writing—review and editing, C.L.; supervision, K.Z. and C.S. All authors have read and agreed to the published version of the manuscript.

**Funding:** This research received no external funding.

**Data Availability Statement:** The original contributions presented in the study are included in the article; further inquiries can be directed to the corresponding authors.

**Acknowledgments:** First of all, We would like to express our appreciation to Stephen J Skinner, for his helpful advice, scientific discussions, and patient guidance. His experience in the solid oxide fuel cell field is invaluable. Next, we would like to thank some research staff at the Imperial College, Richard Sweeney, Mahmoud G Ardakani, Florent Tonus, Zonghao Shen and Duke, for their wonderful collaboration and patient support which is important to our work.

**Conflicts of Interest:** Authors Manyu Chen, Kai Zhu, Jieyu Wang, Sida Liu, Weina Kong, Zifa Ban and Chao Shen were employed by the company Avic Composite Corporation Ltd. The remaining authors declare that the research was conducted in the absence of any commercial or financial relationships that could be construed as a potential conflict of interest.

## References

1. Goodenough, J.B.; Ruiz-Diaz, J.E.; Zhen, Y.S. Oxide-ion conduction in  $\text{Ba}_2\text{In}_2\text{O}_5$  and  $\text{Ba}_3\text{In}_2\text{MO}_8$  ( $M = \text{Ce}, \text{Hf}, \text{or Zr}$ ). *Solid State Ion.* **1990**, *44*, 21–31. [[CrossRef](#)]
2. Ishihara, T.; Matsuda, H.; Takita, Y. Doped  $\text{LaGaO}_3$  perovskite type oxide as a new oxide ionic conductor. *J. Am. Chem. Soc.* **1994**, *116*, 3801–3803. [[CrossRef](#)]
3. Goodenough, J.B. Oxide-ion conductors by design. *Nature* **2000**, *404*, 821–823. [[CrossRef](#)]
4. León-Reina, L.; Losilla, E.R.; Martínez-Lara, M.; Martín-Sedeño, M.C.; Bruque, S.; Núñez, P.; Sheptyakov, D.V.; Aranda, M.A.G. High oxide ion conductivity in Al-doped germanium oxyapatite. *Chem. Mater.* **2005**, *17*, 596–600. [[CrossRef](#)]
5. Li, M.; Pietrowski, M.J.; De Souza, R.A.; Zhang, H.; Reaney, I.M.; Cook, S.N.; Kilner, J.A.; Sinclair, D.C. A family of oxide ion conductors based on the ferroelectric perovskite  $\text{Na}_{0.5}\text{Bi}_{0.5}\text{TiO}_3$ . *Nat. Mater.* **2014**, *13*, 31–35. [[CrossRef](#)] [[PubMed](#)]
6. Kim, J.; Sengodan, S.; Kim, S.; Kwon, O.; Bud, Y.; Kim, G. Proton conducting oxides: A review of materials and applications for renewable energy conversion and storage. *Renew. Sustain. Energy Rev.* **2019**, *109*, 606–618. [[CrossRef](#)]
7. Zhang, W.; Fujii, K.; Niwa, E.; Hagihala, M.; Kamiyama, T.; Yashima, M. Oxide-ion conduction in the Dion–Jacobson phase  $\text{CsBi}_2\text{Ti}_2\text{NbO}_{10-\delta}$ . *Nat. Commun.* **2020**, *11*, 1224. [[CrossRef](#)]
8. Zvonareva, I.; Fu, X.-Z.; Medvedev, D.; Shao, Z. Electrochemistry and energy conversion features of protonic ceramic cells with mixed ionic-electronic electrolytes. *Energy Environ. Sci.* **2021**, *15*, 439–465. [[CrossRef](#)]
9. Gao, Y.; Zhang, M.; Fu, M.; Hu, W.; Tong, H.; Tao, Z. A comprehensive review of recent progresses in cathode materials for Proton-conducting SOFCs. *Energy Rev.* **2023**, *2*, 100038. [[CrossRef](#)]
10. Yuki, N. Proton-Conducting Polymers: Key to Next-Generation Fuel Cells, Electrolyzers, Batteries, Actuators, and Sensors. *ChemElectroChem* **2024**, *2024*, e202300846.
11. Fujii, K.; Esaki, Y.; Omoto, K.; Yashima, M.; Hoshikawa, A.; Ishigaki, T.; Hester, J.R. New Perovskite-Related Structure Family of Oxide-Ion Conducting Materials  $\text{NdBaInO}_4$ . *Chem. Mater.* **2014**, *26*, 2488–2491. [[CrossRef](#)]
12. Fujii, K.; Shiraiwa, M.; Esaki, Y.; Yashima, M.; Kim, S.J.; Lee, S. Improved oxide-ion conductivity of  $\text{NdBaInO}_4$  by Sr doping. *J. Mater. Chem. A* **2015**, *3*, 11985–11990. [[CrossRef](#)]
13. Ishihara, T.; Yan, Y.; Sakai, T.; Ida, S. Oxide ion conductivity in doped  $\text{NdBaInO}_4$ . *Solid State Ion.* **2016**, *288*, 262–265. [[CrossRef](#)]
14. Souza, D.; Chater, R. Oxygen exchange and diffusion measurements: The importance of extracting the correct initial and boundary conditions. *Solid State Ion.* **2005**, *176*, 1915–1920.
15. Kilner; Steele, B.; Ilkov, L. Oxygen self-diffusion studies using negative-ion secondary ion mass spectrometry (SIMS). *Solid State Ion.* **1984**, *12*, 89–97. [[CrossRef](#)]
16. Shannon, R.T. Revised effective ionic radii and systematic studies of interatomic distances in halides and chalcogenides. *Acta Crystallogr. Sect. A Cryst. Phys. Diffr. Theor. Gen. Crystallogr.* **1976**, *32*, 751–767. [[CrossRef](#)]
17. Logan, S.R. The origin and status of the Arrhenius equation. *J. Chem. Educ.* **1982**, *59*, 279. [[CrossRef](#)]
18. Haugsrud, R.; Norby, T. Proton conduction in rare-earth ortho-niobates and ortho-tantalates. *Nat. Mater.* **2006**, *5*, 193–196. [[CrossRef](#)]

**Disclaimer/Publisher’s Note:** The statements, opinions and data contained in all publications are solely those of the individual author(s) and contributor(s) and not of MDPI and/or the editor(s). MDPI and/or the editor(s) disclaim responsibility for any injury to people or property resulting from any ideas, methods, instructions or products referred to in the content.